

Resonant x-ray-scattering study of octahedral tilt ordering in LaMnO_3 and $\text{Pr}_{1-x}\text{Ca}_x\text{MnO}_3$

M. v. Zimmermann, C. S. Nelson, Y.-J. Kim, J. P. Hill, and Doon Gibbs
Physics Department, Brookhaven National Laboratory, Upton, New York 11973-5000

H. Nakao, Y. Wakabayashi,* and Y. Murakami
Photon Factory, Institute of Materials Structure Science, Tsukuba 305-0801, Japan

Y. Tokura[†] and Y. Tomioka
Joint Research Center for Atom Technology (JRCAT), Tsukuba 305-0046, Japan

T. Arima
Institute of Materials Science, University of Tsukuba, Tsukuba 305-8573, Japan

C.-C. Kao
National Synchrotron Light Source, Brookhaven National Laboratory, Upton, New York 11973-5000

D. Casa, C. Venkataraman, and Th. Gog
CMC-CAT, Advanced Photon Source, Argonne National Laboratory, Argonne, Illinois 60439

(Received 15 February 2001; published 19 July 2001)

We report an x-ray-scattering study of octahedral tilt ordering in the manganite series $\text{Pr}_{1-x}\text{Ca}_x\text{MnO}_3$ with $x=0.4$ and 0.25 and in LaMnO_3 . The sensitivity to tilt ordering is achieved by tuning the incident x-ray energy to the L_I , L_{II} , and L_{III} absorption edges of Pr and La, respectively. The resulting energy-dependent profiles are characterized by a dipole-resonant peak and higher-energy fine structure. The polarization dependence is predominantly σ to π and the azimuthal dependence follows a sin-squared behavior. These results are similar to those obtained in recent x-ray-scattering studies of orbital ordering carried out in these same materials at the Mn K edge. They lead to a description of the cross section in terms of Templeton scattering in which the tilt ordering breaks the symmetry at the rare-earth site. The most interesting result of the present work is our observation that octahedral tilt ordering persists above the orbital ordering transition temperatures in all three samples. Indeed, we identify separate structural transitions which may be associated with the onset of orbital and tilt ordering, respectively, and characterize the loss of tilt ordering versus temperature in LaMnO_3 .

DOI: 10.1103/PhysRevB.64.064411

PACS number(s): 75.30.Vn, 61.10.Eq, 64.60.Cn

I. INTRODUCTION

The AMO_3 aristotype is the defining feature of the cubic perovskite structure. It consists of a cubic array of metal-oxygen octahedra centered on a lanthanide ion (A). In the transition metal oxides, the aristotype is generally observed only at high temperatures. At lower temperatures, a variety of distortions of the octahedra may occur, which reduce the cubic symmetry. It is interesting that most, if not all, of the unusual properties exhibited by these materials, including colossal magnetoresistance and high-temperature superconductivity, occur in the lower-temperature range. It remains an open question as to whether these distortions are required for such phenomena to occur.

A prominent example of an octahedral distortion is the Jahn-Teller distortion in the manganites. In specific cases, this involves the lengthening of two Mn-O bonds of the MnO_6 octahedra and the concomitant shortening of four others. It is accompanied by orbital ordering of the occupied Mn $3d$ orbitals. Likewise, charge ordering involves the inhomogeneous localization of electronic charge at Mn sites to form ordered arrays. Both orbital and charge ordering introduce new periodicities into the system and may be accompanied by longitudinal or transverse lattice distortions. Characterizing the charge, orbital and magnetic ordering in transition

metal oxides, and exploring their coupling to the lattice, is an active field of current research.¹⁻³

Another important distortion of the cubic perovskites involves the tilting of the metal-oxygen octahedra. These ordered rotations are well known, having been discussed by Goldschmidt in the 1920s,⁴ and again by Goodenough in the 1950s.⁵ A complete crystallographic treatment of 23 possible tilt patterns has been given by Glazer⁶ and refined more recently by Woodward.^{7,8} The underlying idea is that a small tilt of the octahedra shortens the A -site ion-to-oxygen bond distances, while preserving the length of the metal-oxygen bond—thereby lowering the total energy. A three-dimensional view of one common tilt ordering, the so-called GdFeO_3 distortion, is illustrated in Fig. 1, together with three two-dimensional projections.⁹ It is intriguing that in LaMnO_3 the periodicity of the Mn orbital ordering is the same as that of the octahedral tilt ordering. This raises the questions of whether the tilt ordering is coupled to the orbital ordering, possibly as a precursor, and whether the tilting plays a more important role in the properties of colossal magnetoresistance (CMR) materials than has been recognized to date. In a recent paper, Mizokawa *et al.*¹⁰ addressed these questions in LaMnO_3 and $\text{Pr}_{1-x}\text{Ca}_x\text{MnO}_3$ (hereafter referred to as PCMO), among others. They showed that the GdFeO_3 distortion stabilizes the so-called d -type orbital ordering pattern

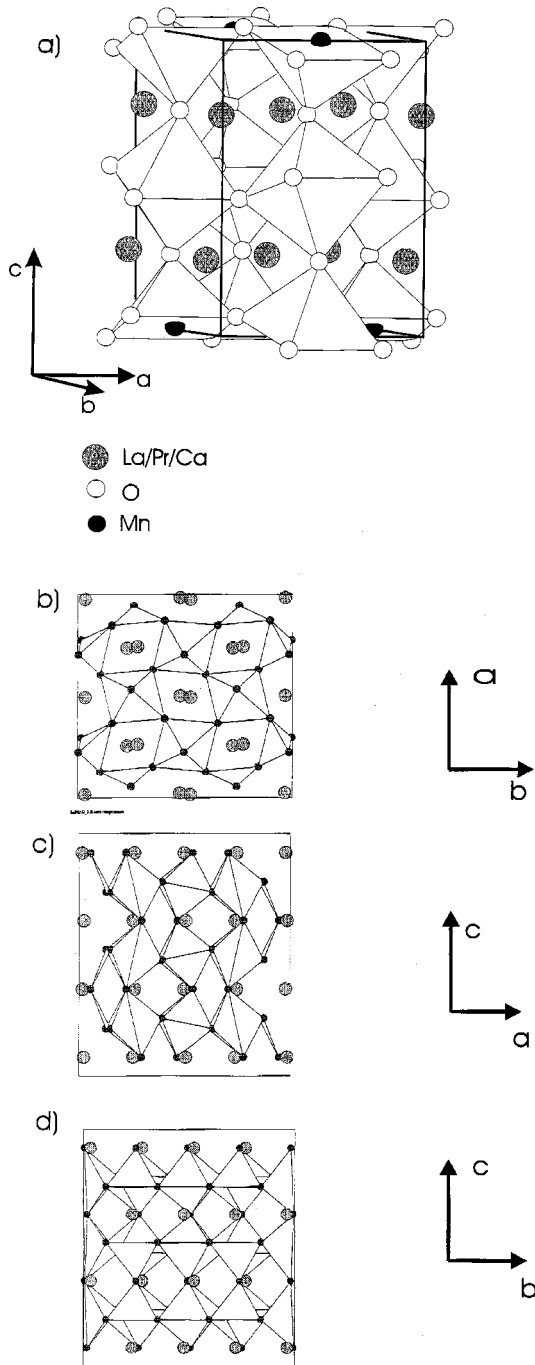


FIG. 1. (a) A three-dimensional view of a perovskite structure including the octahedral tilt ordering associated with the GdFeO_3 -type distortion. (b), (c), and (d) are projections of (a) along orthorhombic c , b , and a axes, respectively (for the particular case of LaMnO_3 at room temperature). Small clear (dark) spheres represent oxygen atoms at the corners (Mn atoms at the center) of the octahedra. Larger spheres represent the A-site ions, which for the materials studied here are either La, Pr, or Ca.

in LaMnO_3 by increasing the hybridization of the La atoms with three of the corner oxygen atoms. However, experimental studies of these effects in manganites have been limited.¹¹

In this paper we discuss x-ray resonant scattering studies of the octahedral tilt ordering observed in LaMnO_3 ,

$\text{Pr}_{0.75}\text{Ca}_{0.25}\text{MnO}_3$, and $\text{Pr}_{0.6}\text{Ca}_{0.4}\text{MnO}_3$. In analogy to recent studies of orbital ordering in which the incident energy is tuned to the Mn K edge,^{12,13,2} we show that in each case it is possible to probe octahedral tilt ordering by tuning the photon energy to the respective La and Pr L absorption edges. Specifically, we report resonant spectra of the tilt ordering at the La and Pr L_I ($2s \rightarrow 6p$), and L_{II-III} ($2p \rightarrow 5d$) edges, including the azimuthal dependence at the Pr L_{II} edge of $\text{Pr}_{0.75}\text{Ca}_{0.25}\text{MnO}_3$. We find that the resonant fine structures at the L_{II} and L_{III} edges are qualitatively similar, involving a main resonant peak and weaker subsidiary peaks, whereas the L_I spectra involve only a single resonance. We believe these differences reflect the electronic structure of the intermediate states; however, a full theoretical analysis including the $5d$ and $6p$ bands is required before quantitative conclusions can be drawn. The polarization dependence of the resonant scattering is predominantly $\sigma \rightarrow \pi$ to within experimental errors, and the azimuthal dependence follows a sin-squared behavior. Both are consistent with simple models of Templeton scattering based on a splitting of the resonant intermediate states.^{14,2,15,13} Where possible, specific comparisons are made with the predictions of Benedetti *et al.*,¹⁶ who have carried out local density approximation (LDA) + U calculations of these effects for LaMnO_3 . No evidence has been found for lattice modulations involving a longitudinal periodic displacement of the A-site ions away from their symmetry positions in LaMnO_3 and $\text{Pr}_{0.75}\text{Ca}_{0.25}\text{MnO}_3$; however, the possibility of a transverse displacement has not yet been explored.

The most interesting results of the present work concern the temperature dependence of the octahedral tilt ordering. In particular, we find that the tilt ordering in LaMnO_3 persists above the orbital ordering transition at ~ 800 K and then disappears at ~ 1000 K. Both the tilt and orbital ordering transitions are associated with corresponding structural transitions of the lattice, which we specify. Interestingly, the line-width of the octahedral tilt ordering is resolution limited below the orbital ordering temperature, but starts to increase about 70 K above it. No evolution of the main peak of the resonant line shapes of the L_{II} and L_I absorption edges was found for temperatures increasing above the orbital ordering transition, which differs from the predictions of Benedetti *et al.*¹⁶

The situation is more complicated in $\text{Pr}_{0.75}\text{Ca}_{0.25}\text{MnO}_3$ for which the structure of the orbital ordering is itself controversial. Although most of the orbital order scattering in this material disappears at about 400 K, coincident with a structural transition, a small peak nevertheless persists at the Mn K edge up to 900 K. In contrast, the intensity of the resonant tilt scattering measured at the Pr L_{II} edge is approximately constant from 10 to 900 K, the highest temperature accessible with the present apparatus. Similarly, there is little change of the resonant line shape at the L_I and L_{II} absorption edges of $\text{Pr}_{0.6}\text{Ca}_{0.4}\text{MnO}_3$, as the temperature is increased through its orbital ordering temperature ($T_{co} \sim 245$ K); nor are there variations of the tilt scattering intensity, correlation length, or periodicity, at least up to about 300 K.

Taken together, these results offer a new probe of octahedral tilt ordering and of its possible coupling to charge and orbital ordering in the pseudocubic perovskites. In the following, we briefly describe the experimental setup and the phase behavior of LaMnO_3 and $\text{Pr}_{1-x}\text{Ca}_x\text{MnO}_3$ before turning to a discussion of our results.

II. EXPERIMENT

The single crystals used in the present experiments were grown by floating zone techniques at JRCAT. (1,0,0) and (0,1,0) surfaces were cut from cylinders of radius ~ 3 mm, and polished with fine emery paper and diamond paste. The mosaic widths of the LaMnO_3 and PCMO samples, as characterized at the (0,2,0) bulk Bragg reflections (in orthorhombic notation), were all about 0.1° [full width at half maximum (FWHM)], as described earlier.^{2,15,17} These values varied by small amounts as the beam was moved across each sample surface, reflecting its mosaic distribution. The growth techniques and basic transport properties have been described in detail elsewhere.^{18–20}

X-ray-scattering experiments were carried out at the National Synchrotron Light Source on bending magnet X22C and wiggler X21 beamlines, and at the Advanced Photon Source on beamline 9ID. X22C is equipped with a bent, toroidal focusing mirror and a Ge(1,1,1) double-crystal monochromator arranged in a vertical scattering geometry. This gives an incident linear polarization of 95% (σ) and an incident energy resolution of between 5 and 10 eV at the Mn K and La and Pr L_I , L_{II} , and L_{III} edges. Two different detector configurations were used. High-momentum transfer resolution scans employed a Ge(1,1,1) crystal, and gave a longitudinal resolution of $4.5 \times 10^{-4} \text{ \AA}^{-1}$ [half width at half maximum (HWHM)] at the respective (0,1,0) reflections and linear polarization analysis of the scattered beam was provided via rotation of a Cu(2,2,0) crystal around the scattered beam direction.²¹ The latter gave longitudinal resolutions of 0.0069 \AA^{-1} and 0.0052 \AA^{-1} (HWHM) in the $\sigma \rightarrow \sigma$ and $\sigma \rightarrow \pi$ geometries, respectively. NSLS Wiggler beamline X21 was equipped with a four-bounce Si(2,2,0) monochromator and a focusing mirror, leading to an incident energy resolution of 0.25 eV. The APS undulator beamline 9ID consists of a double-crystal Si(1,1,1) monochromator, a focusing mirror (coated with Pt), and a flat harmonic rejection mirror. The incident energy resolution was approximately 1.5 eV.

A serious complication associated with the present experiments was our observation that these crystals do not tolerate repeated excursions to high temperatures, 800 K, before changing their properties. The most dramatic of the effects we observed was the loss of long-range orbital order in one of the LaMnO_3 samples after extended cycling above 1000 K and cooling back to room temperature. These effects are common among perovskites and originate in strain relief within individual grains and, perhaps, in oxygen depletion.^{22,23} As a consequence, our ability to double-check all of the results obtained for LaMnO_3 has been limited.

At low temperatures, $\text{Pr}_{0.75}\text{Ca}_{0.25}\text{MnO}_3$ and LaMnO_3 have pseudocubic perovskite structures with orthorhombic symmetry $Pbnm$ (illustrated in Fig. 1). Each Mn atom lies at the

center of an octahedron defined by six oxygen atoms at the corners. Single layers of La or Pr/Ca atoms lie between the layers of octahedra. Both materials are insulating and believed to exhibit an orbitally ordered ground state. The electronic configurations of the $(\text{Mn})^{3+}$ (d^4) ions are (t_{2g}^3, e_g^1) with the t_{2g} electrons localized at the Mn sites. The e_g electrons are hybridized with the oxygen $2p$ orbitals and participate in a cooperative Jahn-Teller distortion of the MnO_6 octahedra. This is believed to lead to a $(3x^2 - r^2) - (3y^2 - r^2)$ zigzag-type of orbital ordering of the e_g electrons with the oxygen displaced along the direction of extension of the e_g orbitals, as has been discussed in detail elsewhere.^{1,2,5} In orthorhombic notation, for which the fundamental Bragg peaks occur at $(0,2k,0)$, with k an integer, the orbital scattering occurs at $(0,2k+1,0)$. Regarding their magnetic structures, $\text{Pr}_{0.75}\text{Ca}_{0.25}\text{MnO}_6$ is ferromagnetic, while LaMnO_3 is an A -type antiferromagnet, below their respective magnetic ordering temperatures.

$\text{Pr}_{0.6}\text{Ca}_{0.4}\text{MnO}_3$ also has a perovskite structure with $Pbnm$ symmetry, but exhibits an insulating CE type, antiferromagnetic ground state at low temperature, including a cooperative Jahn-Teller distortion. The higher Ca doping in this material leads to a large negative magnetoresistance in an applied magnetic field with the metal-insulator transition occurring at about 6 T at low temperature.¹⁹ The ordered phase is accompanied by a second modulation of the lattice arising from an ordering of two different Mn sites, conventionally referred to as Mn^{3+} and Mn^{4+} ions, which occurs in addition to orbital ordering.² In orthorhombic notation, the charge order reflections in $\text{Pr}_{0.6}\text{Ca}_{0.4}\text{MnO}_3$ occur at $(0,2k+1,0)$, whereas the orbital reflections are at $(0,k+1/2,0)$. Note that the orbital period present in the $x=0.4$ sample ($=2b$) differs from that in the $x=0.25$ sample ($=b$) as a result of the charge ordering. Detailed x-ray-scattering studies of the charge and orbital ordering in LaMnO_3 and PCMO have been reported elsewhere.^{2,12,15,17}

In addition to the Jahn-Teller distortion, all three compounds undergo so-called GdFeO₃ distortion, which involves tilting of the MnO_6 octahedra, as shown in Fig. 1. In GdFeO₃ distortion, the four octahedra in the unit cell are rotated by an angle ω around an axis in the (0,1,1) plane. This may be approximated as a compound rotation of the octahedra first about the b axis [Fig. 1(d)] followed by a much smaller rotation about the a axis [Fig. 1(c)]. From the present perspective, it is important to note that the periodicity of the octahedral tilt ordering in LaMnO_3 and $\text{Pr}_{0.75}\text{Ca}_{0.25}\text{MnO}_3$ is identical to that of the orbital ordering (specified above). In contrast, the octahedral tilt ordering in $\text{Pr}_{0.6}\text{Ca}_{0.4}\text{MnO}_3$ has the same period as the charge ordering, which is half that of the orbital ordering. Crystallographic studies of the structure of LaMnO_3 (Refs. 11 and 24) suggest that the octahedral tilting angle is reduced from 16° to 12° , but not eliminated, by increasing the sample temperature from 300 to 800 K. They also suggest that both the oxygen atoms and A -site ions are displaced by octahedral tilting, all the while maintaining $Pbnm$ symmetry. To our knowledge, there are no comparable crystallographic studies of PCMO for the dopings considered here, but qualitative similarities are expected.

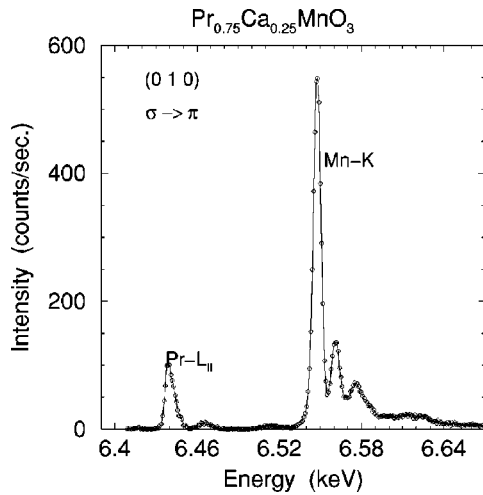


FIG. 2. Scan of the x-ray intensity measured at the (0,1,0) wave vector of $\text{Pr}_{0.75}\text{Ca}_{0.25}\text{MnO}_3$ for incident x-ray energies between 6.4 and 6.64 keV. The Pr L_{II} and Mn K -edge absorption energies are marked. The sample was held at 10 K.

III. RESULTS AND DISCUSSIONS

A. Resonant profiles

Figure 2 shows the energy dependence of the scattering at the (0,1,0) orbital wave vector of $\text{Pr}_{0.75}\text{Ca}_{0.25}\text{MnO}_3$ as the incident x-ray energy is tuned through the Mn K and Pr L_{II} absorption edges. These data were obtained using a polarization analyzer and explicitly resolve the π component of the resonant scattering, consistent with a rotation of the incident linear polarization from σ to π . Referring to the figure, a large resonant signal is visible at $\hbar\omega = 6.547$ keV, reaching about 500 counts/sec near the Mn K edge. In addition, there are two smaller peaks at $\hbar\omega = 6.56$ and 6.575 keV and a broad peak at $\hbar\omega = 6.62$ keV. Remarkably, there is also a resonant feature at the Pr L_{II} edge with $\hbar\omega = 6.44$ keV. It is this latter resonance which is the subject of the present paper.

Detailed scans of the resonant scattering obtained at the orbital wave vectors of $\text{Pr}_{0.75}\text{Ca}_{0.25}\text{MnO}_3$ and LaMnO_3 for incident x-ray energies tuned through the L_I , L_{II} , and L_{III} edges of Pr and La are shown in Figs. 3 and 4, respectively. These data were obtained at the (0,1,0) reflections of each sample using a Ge(1,1,1) analyzer crystal, and thereby combine any σ and π components of the scattering. Similar results for $\text{Pr}_{0.6}\text{Ca}_{0.4}\text{MnO}_3$ (polarization resolved) are shown in Fig. 6, discussed later.

The data for the L_I edges are simplest, consisting in each case of a resonant profile centered near the white line of the fluorescence, with a width of about 10 eV. Fits of the line shapes to squared Lorentzians suggest the possibility of a weak asymmetry with additional intensity at lower energy.³⁶

The profiles of the Pr scattering at the L_{II-III} edges show more fine structure (Fig. 3). In each case, the main resonance occurs 2–3 eV above the inflection point of the fluorescence line, and has a full width of between 6 and 9 eV.²⁵ Fits of the main resonance peaks to squared Lorentzians again suggest that the line shapes are not symmetric, in this case having longer high-energy tails. It is not clear from the data whether this asymmetry reflects an additional excitation channel

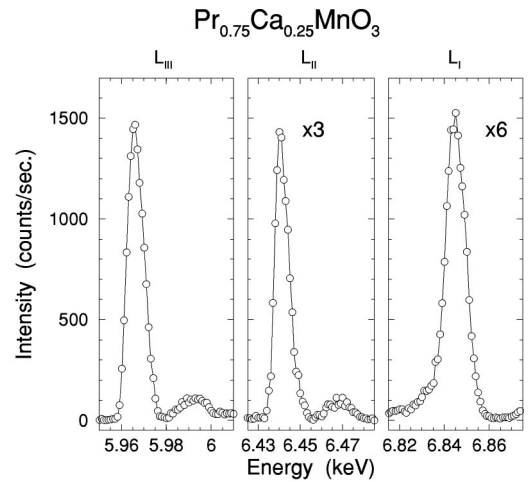


FIG. 3. Scans of the intensity measured at the (0,1,0) wave vector of $\text{Pr}_{0.75}\text{Ca}_{0.25}\text{MnO}_3$ vs incident x-ray energies near the Pr L_{III} , L_{II} , and L_I absorption edges. These data were obtained with a Ge(111) analyzer and so combine any σ and π contributions to the scattering. The sample was held at room temperature in these scans.

(simply adding to the intensity) or instead arises from an interference effect, or from multiple scattering. In addition to the main resonance, there is a second peak occurring about 30 eV above the resonance at both the L_{II} and L_{III} absorption edges. We have ruled out multiple scattering as the origin of these latter peaks and believe that they are of physical interest. Polarization analysis reveals that both the main resonant peak and the second peak 30 eV above it occur predominantly in the σ - π channel. More specifically, we find that the main resonant feature at the Pr L_{II} edge of $\text{Pr}_{0.6}\text{Ca}_{0.4}\text{MnO}_3$ gives a ratio of the σ - π / σ - σ scattering of at least 25.

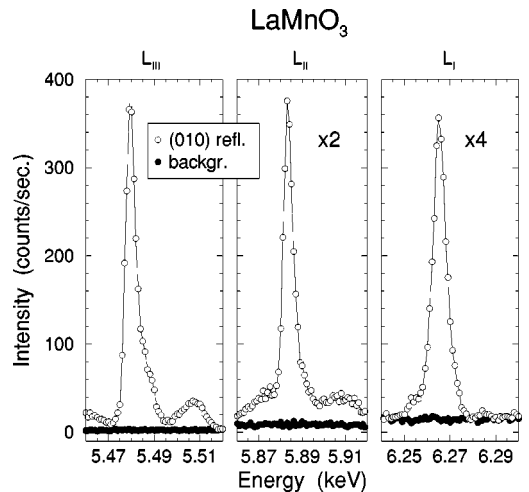


FIG. 4. Scans of the intensity measured at the (0,1,0) wave vector of LaMnO_3 vs incident x-ray energies near the La L_{III} , L_{II} , and L_I absorption edges. Solid circles show energy scans of the background intensity taken at (0.975, 0, 0.033) for comparison. These data were obtained with a Ge(111) analyzer and so combine any σ and π contributions to the scattering. The sample was held at room temperature.

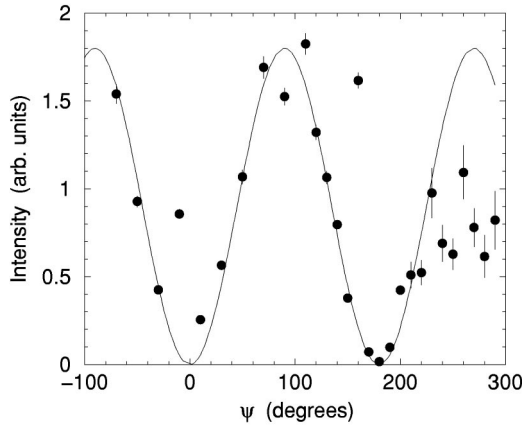


FIG. 5. Azimuthal dependence of the scattering at the (0,1,0) wave vector of $\text{Pr}_{0.75}\text{Ca}_{0.25}\text{MnO}_3$ for incident x-ray energies at the Pr L_{II} absorption edge. The solid line is a fit to the form $A \sin^2 \psi$.

The resonant line shapes obtained at the La L_{II} and L_{III} edges in LaMnO_3 are qualitatively similar to those obtained at the Pr L edges, and are shown in Fig. 4. In each case, the main resonant peak occurs 2–3 eV above the inflection point of the fluorescence and exhibits a slight asymmetry to higher energy. There are additional peaks occurring about 30 eV above the main resonance, similar to those observed in the PCMO samples. As we have not yet adequately characterized the multiple scattering in this sample, we cannot rule it out at this second peak position in LaMnO_3 . Given the similarity of these features with those observed in PCMO, where multiple scattering was ruled out, it is tempting to conclude that it is not a factor here. We suspect, however, that the shoulder located about 10 eV below the L_{II} absorption edges (see Fig. 4) and a broad peak centered at 5.405 keV (whose tail is visible at low energy in the scan of the L_{III} absorption edge) do arise from multiple scattering. These latter details will have to be confirmed in future measurements; however, their outcome will not detract from the main results presented here.

An important feature of the resonant scattering is the dependence of the intensity on azimuthal angle. The azimuthal angle ψ characterizes rotations of the sample about the scattering wave vector and is defined to be zero when the c axis is perpendicular to the scattering plane. A quantitative study of the azimuthal dependence of the L_{II} resonant scattering of $\text{Pr}_{0.75}\text{Ca}_{0.25}\text{MnO}_3$ is shown in Fig. 5. Each data point represents the maximum resonant intensity obtained in the σ - π geometry at the (0,1,0) reflection at a particular azimuthal angle. The data have been normalized by the intensity of the (0,2,0) reflection at that azimuth to correct for small variations due to sample shape. In contrast to normal charge scattering, for which the intensity is independent of the azimuthal angle, the resonant scattering exhibits an oscillation with twofold symmetry. The intensity approaches zero when $\psi=0$ and 180° , similar to the σ - π polarized component of the orbital scattering measured at the Mn K edge. The solid line is a fit to the form $A \sin^2 \psi$, as was also found for the azimuthal dependence of the orbital ordering at the Mn K edge.² We believe that the systematic deviation of the data

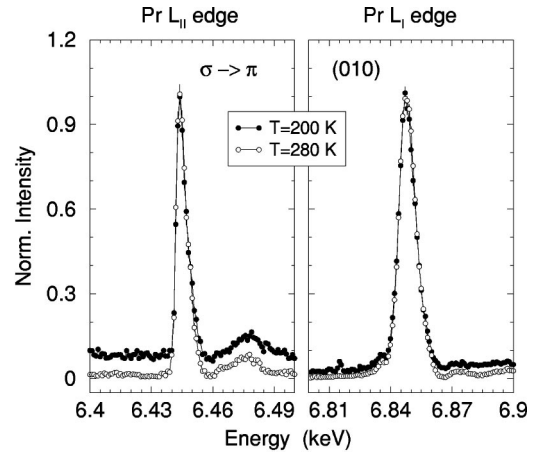


FIG. 6. Intensity of the $\sigma \rightarrow \pi$ component of the resonant scattering obtained at the (0,1,0) wave vector of $\text{Pr}_{0.6}\text{Ca}_{0.4}\text{MnO}_3$ for incident x-ray energies near the Pr L_I and L_{II} absorption edges. Open and solid circles represent data at temperatures above and below the orbital ordering temperature of $T_{co}=245$ K.

from a pure $\sin^2 \psi$ behavior at $\psi > 220^\circ$ probably reflects the inadequacy of our area correction at the (0,2,0) reflection.

Before discussing the Pr scattering in more detail, we first discuss the main peak and fine structure near the Mn K edge (shown in Fig. 2). These features have been observed previously and interpreted in terms of orbital ordering.² Briefly, two kinds of Mn site are distinguishable depending on the local orientation of the e_g electron, as a result of the cooperative Jahn-Teller distortion. The resonant scattering observed at the orbital wave vector may then be thought of as Templeton scattering arising from the anisotropic charge distribution induced by orbital ordering.^{14,26} In the dipole approximation, the resonance corresponds to a $1s \rightarrow 4p$ transition at the metal site. In the simplest model, the sensitivity to orbital ordering arises from the splitting of the Mn $4p$ levels as a result of the $3d$ ordering. Discussion of the microscopic origin of the splitting, however, has been controversial^{13,27–30,2,16,31} with both Coulomb- and Jahn-Teller-based descriptions proposed. Insofar as we are aware, the experimental data obtained to date do not distinguish either approach conclusively, and this remains an open question.

Regardless of the origin of the splitting, the resonant scattering at the Mn K edge reflects the symmetry of the orbital ordering through the redistribution of local charge density (and subsequent perturbation of the electron energy levels) at the Mn^{3+} sites, consistent with the space group. It follows that the peak positions and widths measure the orbital periodicity and correlation lengths, respectively. A key feature of this type of resonant scattering at a (0, k ,0) reflection in LaMnO_3 and PCMO is that the azimuthal dependence of the intensities follows a $\sin^2 \psi$ dependence. In addition, the polarization of the incident beam is rotated from σ to π . Full details of these effects may be found elsewhere, including a generalization to the orbital ordering of the t_{2g} levels and to other geometries.^{2,12,13,15,30}

Returning to the Pr resonance, there are at least two possible sources of this scattering. One is that it results from

orbital ordering of the partially occupied Pr $4f$ levels, with a periodicity equal to the Mn $3d$ orbital order. Such antiferro-quadrupolar ordering has recently been observed in the Dy $4f$ levels of DyB₂C₂ at the Dy L_{III} edge.^{32,33} However, this cannot be the origin of the similar effects observed in LaMnO₃, since La lacks $4f$ electrons. A second possibility is that it originates in the differing kinds of Pr environment that exist within the unit cell. While all Pr sites are crystallographically equivalent [resulting in the (0,1,0) being forbidden in $Pbnm$ symmetry], there are in fact two different local Pr environments created by the surrounding oxygens in the tilted phase. These are simply illustrated in Fig. 1. Conventional x-ray scattering is insensitive to such differences; however, at an absorption edge the Pr scattering factor transforms from a scalar to a tensor, reflecting the anisotropies of the resonant ion.^{14,26} The tensors at the two Pr sites are inequivalent, and the (0,1,0) reflection becomes allowed, thereby giving rise to Templeton scattering. Since these two environments result from the tilting of the oxygen octahedra, it follows that the resonant intensity is a measure of the octahedral tilt ordering, with the width of the scattering in reciprocal space providing information on the correlation length of the tilt ordering and its position giving the periodicity.

We therefore interpret the resonant scattering at the La and Pr L edges discussed above as Templeton scattering associated with the anisotropic charge distribution induced by octahedral tilt ordering and consistent with the $Pbnm$ space group. The energies of the resonances in each case suggest dipole excitations coupling $2p_{3/2} \rightarrow 5d_{3/2,1/2}$, $2p_{1/2} \rightarrow 5d_{3/2}$, and $2s \rightarrow 6p$ states for the L_{III} , L_{II} , and L_I absorption edges, respectively. We speculate that the splitting δ_0 in the intermediate states needed for the resonant cross section to give a nonzero intensity originates in the crystal field splitting of the appropriate states at the Pr and La sites following tilting of the octahedra. Given a splitting δ_0 , the same arguments which were used to describe the Mn K -edge resonant scattering at the orbital wave vector may then be applied to describe the scattering from the tilt ordering, and naturally lead to both a sin-squared dependence on the azimuthal angle and a rotated (σ - π) final polarization, as observed. The differences between the resonant L_{II-III} and L_I line shapes—in particular, the apparent absence of higher-energy fine structure at the L_I edge—probably reflect the differing densities of states of the $5d$ and $6p$ intermediate states, respectively. Clarifying this point will require more detailed band-structure calculations.

It is interesting to compare these results with the predictions of Benedetti *et al.*,¹⁶ who have carried out LDA+U calculations of the resonant scattering expected at the La edges of LaMnO₃ in the presence of both orbital and tilt ordering. The main features observed in our data are predicted, including a dipole resonance, a rotated (σ - π) polarization dependence, and sin-squared azimuthal dependence. Our x-ray results also show subsidiary peaks at higher energy, which are qualitatively consistent with the predictions, although the observed peaks fall ~ 10 eV higher than is predicted. These calculations support our identification of the resonant scattering at the La and Pr edges as being associated with the tilt ordering.

A fascinating question concerns the possibility that the orbital ordering of the Mn e_g electrons (and concomitant Jahn-Teller distortion) might also contribute to the resonant scattering at the La and Pr edges through hybridization of the oxygen $2p$ states with the $5d$, $6p$, and $3d$ states of the La/Pr and Mn, respectively. Indeed, the work of Benedetti *et al.* on LaMnO₃ (Ref. 16) suggests that the resonant profile calculated by including only the effects of tilt ordering shifts to slightly lower energy when orbital ordering is subsequently included. We have tested this prediction in Pr_{0.6}Ca_{0.4}MnO₃ and LaMnO₃ by measuring the resonant profiles of the tilt ordering at the Pr L_I and L_{II} edges and at the La L_I edge for temperatures above and below their respective orbital ordering temperatures. Figures 6(a) and 6(b) show the energy dependence of the resonant scattering of Pr_{0.6}Ca_{0.4}MnO₃ obtained at the Pr L_I and L_{II} absorption edges. The data were measured at the (0,1,0) reflection, which for this doping is coincident with a charge order reflection. In order to discriminate against the contribution of the charge ordering, which is predominantly σ - σ polarized,² these data were obtained in a σ - π geometry using the polarization analyzer. Open circles show the results obtained below the orbital ordering temperature at 200 K and solid circles show the data obtained above at 280 K. ($T_{co}=245$ K in this sample.) The main features of the resonant profiles discussed above for Pr_{0.75}Ca_{0.25}MnO₃, including the slight asymmetries and additional fine structure, are reproduced at the higher temperature. More importantly, from the perspective of the theory of Benedetti *et al.*,¹⁶ no changes in the L -edge line shapes are observed with increasing temperature through the orbital ordering transition. From this we conclude that the main features of the L -edge resonant profiles reported here originate in octahedral tilt ordering, and that any contributions to the L -edge resonances arising from the Mn orbital order, e.g., from changes of the La/Pr hybridization with the oxygen motion, are too small to be detected, at least at the present experimental signal rates.

Qualitatively similar results were also obtained at the La L_I edge of LaMnO₃ for temperatures above and below its orbital ordering temperature.³⁷

B. Temperature dependence

The temperature dependence of the resonant intensity of the octahedral tilt ordering obtained at the La L_I absorption edge of LaMnO₃ is shown by the open circles in Fig. 7(a). For comparison, solid circles show the temperature dependence of the resonant intensity of the orbital ordering obtained at the Mn K edge, which is qualitatively consistent with earlier published results.^{15,38} Each data point represents the peak intensity taken from a scan through the (1,0,0) reflection obtained in a high-resolution mode using a Ge(1,1,1) analyzer. All of the data were obtained using a high-temperature oven. Referring to the figure, the La L_I and Mn K resonant intensities are both approximately constant between 300 and 700 K, above which temperature both begin to decrease. The intensities at the La L_I and Mn K edges then fall abruptly to near zero at about 800 K, which corresponds to an orthorhombic-to-orthorhombic structural phase transi-

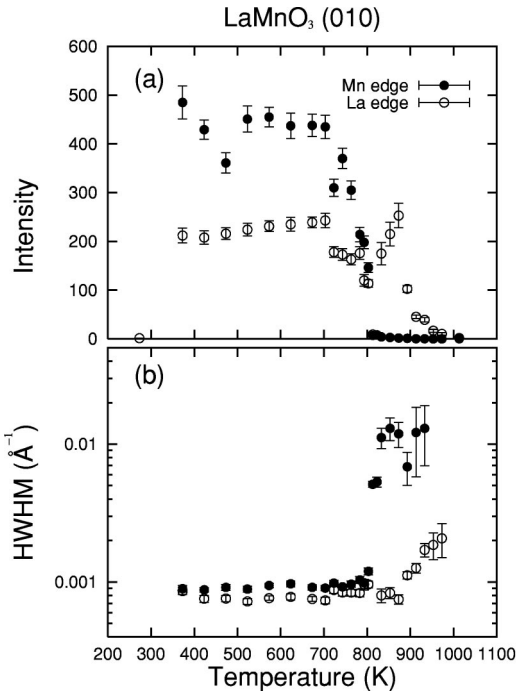


FIG. 7. (a) Temperature dependence of the resonant scattering obtained at the $(0,1,0)$ wave vector of LaMnO_3 at the La L_{II} (open circles), and Mn K (solid circles) absorption edges. (b) Corresponding plot of the half widths at half maxima plotted on a logarithmic scale.

tion ($O' \rightarrow O$). No significant Mn-resonant scattering was observed at the $(0,1,0)$ position of the low-temperature orthorhombic structure (O') at any temperature above 800 K, although a weak, broad peak, consistent with orbital fluctuations, was observed. The intensity of this diffuse scattering falls gradually with increasing temperature and disappears above 1000 K. A strong La-resonant peak reappears above 800 K, but is located at the $(0,1,0)$ position of the high-temperature orthorhombic phase O (open circles). The intensity of the La-resonant scattering in the high-temperature phase increases with temperature until about 870 K, and then decreases again until it disappears at about 1000 K. This suggests that the tilt ordering is preserved within the new lattice, consistent with the results of powder diffraction studies¹¹ (which also report a reduced average tilt angle). It follows that the temperature dependences of the tilt and orbital ordering are distinctly different, with the octahedral tilting persisting to higher temperatures.

The temperature dependences of the corresponding HWHM are plotted on a logarithmic scale for the Mn- and La-resonant scattering in Fig. 7(b). These are proportional to the inverse correlation lengths of the Mn orbital and tilt order, respectively. For temperatures below about 800 K, the widths of both the orbital and tilt scattering are consistent with the resolution, implying correlation lengths of 1000 Å or greater. Above 800 K, the half width of the orbital scattering abruptly broadens by a factor of 10 [see Fig. 7(b)], corresponding to correlation lengths of about ~ 100 Å. The half width of the tilt scattering, however, remains constant up to about 870 K, at which temperature the tilt intensity begins

to decrease. Above this temperature, the width increases continuously. No significant broadening was observed at the $(0,2,0)$ bulk Bragg peak over the entire temperature range.

On the basis of these results, we associate the orthorhombic-to-orthorhombic transition at 800 K with the destruction of long-ranged orbital ordering in LaMnO_3 , in agreement with earlier conclusions.^{15,11} Explicit measurements of the bulk $(2,0,0)$ intensities and positions versus temperature reveal the collapse of the a and b lattice constants to nearly equal values at this temperature, consistent with the appearance of a pseudocubic phase.¹¹ We associate the broad scattering which occurs at the orbital wave vector above 800 K with critical orbital fluctuations, such as have been observed earlier in PCMO for $x=0.4$ and 0.5 .^{17,2} It is interesting that the full widths do not continuously broaden above 800 K, but remain approximately constant, reminiscent of studies of polaron correlations in PCMO and LCMO.³⁴ Accompanying the loss of orbital ordering at 800 K is the apparent loss of octahedral tilt ordering in the low temperature O' phase; however, the tilt ordering reappears in the high-temperature O phase with resolution-limited line-widths. It persists until about 870 K, when the intensities and the correlation lengths start to decrease. Octahedral tilt ordering disappears at ~ 1000 K, corresponding to a structural transition to a rhombohedral phase.¹¹ The fact that the octahedral tilting achieves long-range order at temperatures above the orbital ordering transition appears consistent with the conclusion of Mizokawa *et al.*¹⁰ that the GdFeO_3 distortion stabilizes one type of orbital ordering in LaMnO_3 in preference to another, and suggests that octahedral tilt ordering may serve as a precursor to orbital ordering. It raises the general question of the nature of the coupling between the tilt ordering and the other degrees of freedom in these systems—especially between the orbital and tilt ordering.

The temperature dependence of the intensities of the tilt ordering in $\text{Pr}_{0.75}\text{Ca}_{0.25}\text{MnO}_3$, as obtained at the Pr L_{II} edge, is shown by the solid circles in Fig. 8(a). Open circles represent the temperature dependence of the intensity of the orbital scattering obtained at the Mn K edge and have been published previously.² As above, each data point corresponds to the peak intensity resulting from a scan through the $(0,1,0)$ reflection, which is the orbital wave vector in this sample. The data were obtained using a dispex at low temperatures and an oven at high temperature. The data sets were then scaled to be equal at 300 K. As may be seen from the figure, the Pr-resonant intensities are approximately constant over the entire range accessible between 10 and 900 K. In contrast, the temperature dependence of the orbital scattering as measured at the Mn K edge is approximately constant between 10 and 200 K, and then decreases between 200 and 400 K with a long tail extending up to about 850 K. High-momentum transfer resolution measurements made at both the Pr L_{II} and the Mn K absorption edges show that the peak widths of the Pr and Mn scattering remain approximately constant below 900 K, corresponding to correlation lengths of ~ 1000 Å or greater in each case [see Fig. 8(b)]. It is natural to associate the decrease of the resonant orbital scattering between 200 and 400 K with the orthorhombic struc-

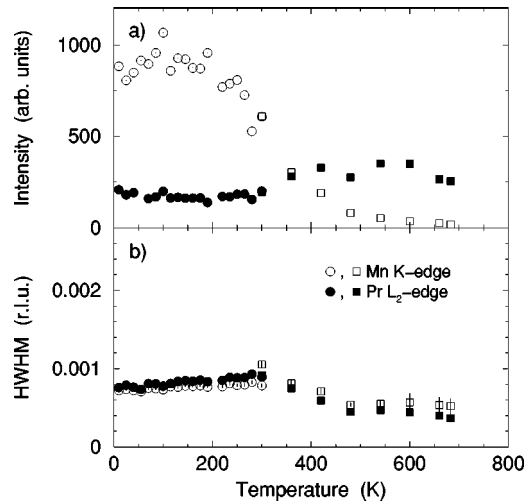


FIG. 8. (a) Temperature dependence of the resonant scattering obtained at the (0,1,0) wave vector of $\text{Pr}_{0.75}\text{Ca}_{0.25}\text{MnO}_3$ at the Pr L_{II} (open symbols) and Mn K (solid symbols) absorption edges. (b) Corresponding plot of the half width at half maxima.

tural transition reported by Jirak *et al.*³⁵ at about 400 K. The data also suggest a small decrease in width for temperatures greater than ~ 400 K. Unfortunately, the high-temperature limit of our oven prevented exploring the possible loss of octahedral tilt ordering above 900 K in this sample.

Similar studies of the orbital and tilt scattering were carried out in $\text{Pr}_{0.6}\text{Ca}_{0.4}\text{MnO}_3$ at selected temperatures between 200 and 300 K. There is a discontinuous change in the lattice constants associated with the loss of orbital ordering at $T_{co} = 245$ K, but neither a decrease in intensity nor a broadening of the resonant peaks associated with the tilt ordering was observed. As with PCMO ($x=0.25$), we were not able to reach the octahedral tilt ordering transition at high temperatures, and are again unable to make quantitative comparisons with LaMnO_3 . Additional experiments on these and other samples will clearly be required before these intriguing results can be understood, especially at elevated temperatures.

IV. CONCLUSIONS

We have presented a detailed study of the x-ray resonant scattering present at the octahedral tilting wave vector of $\text{Pr}_{1-x}\text{Ca}_x\text{MnO}_3$ for $x=0.25$ and 0.4 and of LaMnO_3 for incident x-ray energies tuned to the Pr and La L_I , L_{II} , and L_{III} absorption edges, respectively. We show first that it is possible to characterize the structure and temperature dependence of octahedral tilt ordering in manganites using x-ray resonant techniques, analogously to recent studies of Mn orbital ordering. The energy dependence of the line shapes is characterized by a main resonant peak near the inflection point of the fluorescence in each case, consistent with dipole excitations. Specifically, these are $2p_{3/2} \rightarrow 5d_{5/2,3/2}$, $2p_{1/2}$

$\rightarrow 5d_{3/2}$, and $2s \rightarrow 6p$ for the L_{III} , L_{II} , and L_I absorption edges, respectively. In addition, the L_{II} - and L_{III} -edge spectra exhibit fine structure peaks about 30 eV higher in energy. The polarization dependence of the resonant tilt scattering is found to be (σ - π) to within the accuracy of our measurements, while the azimuthal dependence exhibits a sinusoidal variation. Both are consistent with the expectations of Templeton scattering at this wave vector and for this space group. We interpret these results in terms of a simplified model of the resonant cross section in which the resonant d and p states are split by the local crystal field in analogy to a model proposed for Mn orbital ordering. More accurate band-structure calculations of the cross section of resonant scattering from octahedral tilt ordering by Benedetti *et al.*¹⁶ reproduce qualitative features of the experimental results, including the main dipole resonance and fine structure, together with the polarization and azimuthal dependence. However, we are not able to observe any modification of the line shape upon orbital ordering, in contrast to theoretical predictions.

On the basis of our temperature-dependent studies, it was possible to associate the disappearance of the orbital and tilt scattering at higher temperatures with known structural transitions. Intriguingly, we find that the octahedral tilting in LaMnO_3 is resolution limited (corresponding to domains in excess of 1000 Å) in the presence of orbital ordering, but gradually disorders beginning at temperatures about 70 K above the orbital order transition, until octahedral tilt order is lost at 1000 K. Similar behavior was not observed in the Pr-based materials, at least over the limited range of temperature available with the present apparatus. Further studies at higher temperatures nearer the octahedral tilt order transition are required before direct comparisons with LaMnO_3 are possible. Taken together these results show that it is possible to study octahedral tilt ordering in perovskites using x-ray resonant scattering techniques, and they raise the question of the nature of the coupling between tilt and orbital ordering.

ACKNOWLEDGMENTS

We acknowledge helpful conversations with M. Blume, G.A. Sawatzky, T. Vogt, and P. Woodward. The work at Brookhaven, both in the Physics Department and at the NSLS, was supported by the U.S. Department of Energy, Division of Materials Science, under Contract No. DE-AC02-98CH10886. Support from the Ministry of Education, Science and Culture, Japan, by the New Energy and Industrial Technology Development Organization (NEDO), and by the Core Research for Evolution Science and Technology (CREST) is also acknowledged. Work at the CMC beamlines is supported, in part, by the Office of Basic Energy Sciences of the U.S. Department of Energy and by the National Science Foundation, Division of Materials Research. Use of the Advanced Photon Source was supported by the Office of Basic Energy Sciences of the U.S. Department of Energy under Contract No. W-31-109-Eng-38.

- *Also at Department of Physics, Faculty of Science and Technology, Keio University, Yokohama 223-8522, Japan.
- †Also at Department of Applied Physics, University of Tokyo, Tokyo 113-8656, Japan.
- ¹J. Orenstein and A. J. Millis, *Science* **288**, 468 (2000).
- ²M. v. Zimmermann, C. S. Nelson, J. P. Hill, D. Gibbs, M. Blume, D. Casa, B. Keimer, Y. Murakami, C.-C. Kao, C. Venkataraman, T. Gog, Y. Tomioka, and Y. Tokura, *Phys. Rev. B* (to be published).
- ³Y. Tokura, in *Colossal Magnetoresistance Oxides*, edited by Y. Tokura (Gordon and Breach, London, 1999).
- ⁴V. M. Goldschmidt, *Naturwissenschaften* **14**, 477 (1926).
- ⁵J. B. Goodenough, *Phys. Rev.* **100**, 555 (1955).
- ⁶A. M. Glazer, *Acta Crystallogr., Sect. B: Struct. Crystallogr. Cryst. Chem.* **28**, 3384 (1972).
- ⁷P. M. Woodward, *Acta Crystallogr., Sect. B: Struct. Sci.* **53**, 32 (1997).
- ⁸P. M. Woodward, *Acta Crystallogr., Sect. B: Struct. Sci.* **53**, 44 (1997).
- ⁹In the Glazer notation (Ref. 6), this structure is obtained by rotations about the cubic axes with a pattern $a^+b^-b^-$, that is, one axis distinguished from the other two by having in-phase rotations of the octahedra along that axis. In $Pbnm$ notation, this axis is the c axis. The net effect of these rotations is mostly a rotation about the orthorhombic b axis, Fig. 1.
- ¹⁰T. Mizokawa, D. I. Khomskii, and G. A. Sawatzky, *Phys. Rev. B* **60**, 7309 (1999).
- ¹¹J. Rodriguez-Carvajal, M. Hennion, F. Moussa, A. H. Moudden, L. Pinsard, and A. Revcolevschi, *Phys. Rev. B* **57**, R3189 (1998).
- ¹²Y. Murakami, H. Kawada, H. Kawata, M. Tanaka, T. Arima, Y. Moritomo, and Y. Tokura, *Phys. Rev. Lett.* **80**, 1932 (1998).
- ¹³S. Ishihara and S. Maekawa, *Phys. Rev. Lett.* **80**, 3799 (1998).
- ¹⁴D. H. Templeton and L. K. Templeton, *Acta Crystallogr., Sect. A: Cryst. Phys., Diffr., Theor. Gen. Crystallogr.* **36**, 237 (1980).
- ¹⁵Y. Murakami, J. P. Hill, D. Gibbs, M. Blume, I. Koyama, M. Tanaka, H. Kawata, T. Arima, Y. Tokura, K. Hirota, and Y. Endoh, *Phys. Rev. Lett.* **81**, 582 (1998).
- ¹⁶P. Benedetti, J. V. D. Brink, E. Pavarini, A. Vigliante, and P. Wochner, *Phys. Rev. B* **63**, 060408 (2001).
- ¹⁷M. v. Zimmermann, J. P. Hill, D. Gibbs, M. Blume, D. Casa, B. Keimer, Y. Murakami, Y. Tomioka, and Y. Tokura, *Phys. Rev. Lett.* **83**, 4872 (1999).
- ¹⁸Y. Okimoto, Y. Tomioka, Y. Onose, Y. Otsuka, and Y. Tokura, *Phys. Rev. B* **57**, R9377 (1998).
- ¹⁹Y. Tomioka, A. Asamitsu, H. Kuwahara, Y. Moritomo, and Y. Tokura, *Phys. Rev. B* **53**, 1689 (1996).
- ²⁰Y. Tokura and Y. Tomioka, *J. Magn. Magn. Mater.* **200**, 1 (1999).
- ²¹D. Gibbs, M. Blume, D. R. Harshman, and D. B. McWhan, *Rev. Sci. Instrum.* **60**, 1655 (1988).
- ²²T. Vogt (private communication).
- ²³E. Granado, J. A. Sanjurjo, C. Rettori, J. J. Neumeier, and S. B. Oseroff, *Phys. Rev. B* **62**, 11304 (2000).
- ²⁴Q. Huang, A. Santoro, J. W. Lynn, R. W. Erwin, J. A. Borchers, J. L. Peng, and R. L. Greene, *Phys. Rev. B* **55**, 14 987 (1997).
- ²⁵The measured full widths at the L_{II} absorption edge were 6 eV for the PCMO ($x=0.4$) and LaMnO_3 samples and 7.5 eV for the PCMO ($x=0.25$) sample. The L_{III} full widths were 6 eV for the LaMnO_3 and 9 eV for the PCMO ($x=0.25$).
- ²⁶M. Blume, in *Resonant Anomalous X-ray Scattering*, edited by C. S. G. Materlick and F. Fisher (North-Holland, Amsterdam, 1996).
- ²⁷M. Fabrizio, M. Altarelli, and M. Benfatto, *Phys. Rev. Lett.* **80**, 3400 (1998).
- ²⁸I. S. Elfimov, V. I. Anisimov, and G. A. Sawatzky, *Phys. Rev. Lett.* **82**, 4264 (1999).
- ²⁹M. Benfatto, Y. Joly, and C. R. Natoli, *Phys. Rev. Lett.* **83**, 636 (1999).
- ³⁰S. Ishihara and S. Maekawa, *Phys. Rev. B* **58**, 13 442 (1998).
- ³¹M. Takahashi, J. Igarashi, and P. Fulde, *J. Phys. Soc. Jpn.* **68**, 2530 (1999).
- ³²K. Hirota, N. Oumi, T. Matsumura, H. Nakao, Y. Wakabayashi, Y. Murakami, and Y. Endoh, *Phys. Rev. Lett.* **84**, 2706 (2000).
- ³³Y. Tanaka, T. Inami, T. Nakamura, H. Yamachi, H. Onodera, K. Ohosyama, and Y. Yamaguchi, *J. Phys.: Condens. Matter* **11**, L505 (1999).
- ³⁴C. S. Nelson, M. v. Zimmermann, J. P. Hill, D. Gibbs, V. Kiryukhin, T. Y. Koo, S.-W. Cheong, D. Casa, B. Keimer, T. Gog, and C. T. Venkataraman, cond-mat/0011502 (unpublished).
- ³⁵Z. Jirak, S. Krupica, Z. Simsa, M. Dlouha, and S. Vratilav, *J. Magn. Magn. Mater.* **53**, 153 (1985).
- ³⁶Both samples also show additional, broad peaks between ~ 50 and 80 eV above the L_I edge (not shown). Explicit tests of these latter peaks for multiple scattering were carried out for both PCMO samples by repeating the energy scans at several different azimuths. These tests showed that the broad peaks above the edge arise from multiple scattering. We suspect that the same is true for the LaMnO_3 but have not yet carried out such explicit tests.
- ³⁷A surprising additional result in this sample, however, involved the observation of a continuous shift of the second peak at about 30 eV above the main resonance with increasing temperature. In particular, for temperatures increasing from about 650 K to 800 K, this second resonant peak increased its position by ~ 15 eV. We suspect that multiple scattering or some other artifact, such as oxygen depletion, may be the origin of this effect; however, more systematic tests will require a new sample.
- ³⁸E. Pollert, S. Krupica, and E. Kuzmicova, *J. Phys. Chem. Solids* **43**, 1137 (1982).